

# A Fourier-Based Approach to the Angiographic Assessment of Flow Diverter Efficacy in the Treatment of Cerebral Aneurysms

Tobias Benz\*, Markus Kowarschik, Jürgen Endres, Thomas Redel, Stefanie Demirci, and Nassir Navab

**Abstract**—Flow diversion is an emerging endovascular treatment option for cerebral aneurysms. Quantitative assessment of hemodynamic changes induced by flow diversion can aid clinical decision making in the treatment of cerebral aneurysms. In this article, besides summarizing past key research efforts, we propose a novel metric for the angiographic assessment of flow diverter deployments in the treatment of cerebral aneurysms. By analyzing the frequency spectra of signals derived from digital subtraction angiography (DSA) series, the metric aims to quantify the prevalence of frequency components that correspond to the patient-specific heart rate. Indicating the decoupling of aneurysms from healthy blood circulation, our proposed metric could advance clinical guidelines for treatment success prediction. The very promising results of a retrospective feasibility study on 26 DSA series warrant future efforts to study the validity of the proposed metric within a clinical setting.

**Index Terms**—Cerebral aneurysm, digital subtraction angiography, flow diversion, frequency analysis, power spectrum.

## I. INTRODUCTION

CEREBRAL aneurysms are pathological dilatations of brain vessels that carry the risk of rupture. Aneurysm rupture leads to subarachnoid hemorrhage, a devastating event that leads to death in the majority of cases and leaves about one third of all survivors in need of lifelong care [1]. Even though nontraumatic subarachnoid hemorrhage accounts for only a small portion of stroke mortality, the loss of productive life years is as large as in ischemic stroke, the most common type of stroke [2].

Manuscript received March 14, 2014; accepted April 21, 2014. Date of publication April 29, 2014; date of current version August 28, 2014. *Asterisk indicates corresponding author.*

\*T. Benz is with the Chair for Computer Aided Medical Procedures, Department of Computer Science, Technische Universität München, 80333 Munich, Germany (e-mail: benz@cs.tum.edu).

M. Kowarschik is with Angiography and Interventional X-Ray Systems, Siemens AG, Healthcare Sector, 91301 Forchheim, Germany, and also with the Chair for Computer Aided Medical Procedures, Department of Computer Science, Technische Universität München, 80333 Munich, Germany.

J. Endres is with the Pattern Recognition Lab, Department of Computer Science, Friedrich-Alexander-Universität Erlangen-Nürnberg, 91054 Erlangen, Germany.

T. Redel is with Angiography and Interventional X-Ray Systems, Siemens AG, Healthcare Sector, 91301 Forchheim, Germany.

S. Demirci and N. Navab are with the Chair for Computer Aided Medical Procedures, Department of Computer Science, Technische Universität München, 80333 Munich, Germany.

Color versions of one or more of the figures in this paper are available online at <http://ieeexplore.ieee.org>.

Digital Object Identifier 10.1109/TMI.2014.2320602

Today, a variety of treatment options are available for the clinical management of cerebral aneurysms. The most common are aneurysm clipping [3], a surgical therapy in which a small metal clip is placed across the aneurysm neck, and coil embolization [4], an endovascular procedure in which the aneurysm sac is packed with detachable coils. Aneurysm clipping offers the highest long-term patency rates while the associated risk of treatment is lower in coil embolization. The main shortcomings of coil embolization are high recanalization rates, the persistence of mass effects, and thromboembolic complications due to coil migration into the parent vessel, especially in aneurysms with unfavorable anatomy (e.g., wide-necked aneurysms) [5]. To prevent coil migration and allow dense packing of coils, coil embolization can be conducted through a wide-meshed stent which is placed across the neck of the aneurysm [6].

Flow diversion is an emerging endovascular treatment option for cerebral aneurysms that offers a number of advantages over traditional therapeutic strategies. In particular for aneurysms previously thought to be untreatable, flow diversion has led to remarkable results [7]. Flow diversion aims to cure aneurysms by remodelling the diseased vessel segment that an aneurysm originates from. At least one purpose-designed stent with low porosity and high pore density (called a flow diverter, FD) is placed inside the parent artery across the orifice of the aneurysm. Once in place, the FD acts by mechanical, physiological, and biological means. On a mechanical level, the FD redirects blood flow away from the aneurysm neck such that it remains in the parent artery, slowing down flow inside the aneurysm and thus reducing shear stresses [8]–[10]. In addition, an FD can also favorably change the configuration of the parent artery, thereby changing the aneurysm inflow zone [11]. Physiologically, the disruption of intra-aneurysmal flow promotes blood clotting and thrombus formation. The blood clot is expected to grow in size and eventually occlude the entire aneurysm. As soon as the clot is mature, it may turn into scar tissue and subsequently retract. Thus, a high degree of resolution of the aneurysm mass can be achieved. Aside from these mechanical and physiological effects, an FD also induces a biological process. The surface of the FD offers a scaffold for tissue overgrowth, supporting the development of neointima and endothelial tissue. Eventually, the abnormal opening of the vessel wall is expected to be completely closed, thereby restoring the anatomy of the parent vessel and excluding the aneurysm from the circulation of blood.

The underlying principle of flow diversion for intracranial aneurysm treatment is simple and elegant in nature. Yet, it

TABLE I  
OVERVIEW OF THE METHODS REVIEWED IN SECTION II

Method	Proposed by	Description	References
SMART scale	Grunwald <i>et al.</i>	Five-point grading scale	[13]
Evaluation of aneurysmal blood flow	Tenjin <i>et al.</i>	TCC-based; Model fit: gamma-variate function; Curve parameters: TTP, $T_{1/2}$ , MTT	[14]
Evaluation of aneurysmal blood flow	Asakura <i>et al.</i>	TCC-based; Model fit: two-exponential function; Parameter: exponential parameter of wash-in part	[15]
Analysis of contrast settling	Wang <i>et al.</i>	TCC-based; Model fits: polynomial function for peak region, exponential function for wash-out part; Curve parameters: maximum value and WOT	[16], [17]
Normalized Time-Density Curves	Ionita <i>et al.</i>	TCC-based; Normalized by amount and velocity of contrast agent; Model fits: linear fit to rising part, exponential fit to trailing part; Curve parameters: maximum value, TTP, MTT, IF, and WOT	[18], [19], [20]
Curve parameters extracted from washout-fit	Struffert <i>et al.</i>	TCC-based; Model fit: washout-function as proposed by Sadasivan <i>et al.</i> ; Curve parameters: TTP, FWHM, IF, and OF	[21]
Washout coefficient	Sadasivan <i>et al.</i>	TCC-based; Model fit: purpose-designed function based on fluid-dynamics; Parameter: Washout coefficient (derived from best-fit values)	[22], [23], [24], [25], [26], [27]
Intra-aneurysmal flow to arterial flow ratio	Jou <i>et al.</i>	TCC-based; Normalized over vessel volume; Parameter: f-number (ratio of intra-aneurysmal flow to flow in parent artery)	[28]
Mean aneurysm flow amplitude	Pereira <i>et al.</i>	OF-based; First-order div-curl regularization; Parameters: average estimated intra-aneurysmal blood speed; Normalized by estimated volumetric flow in parent artery	[29]
Flow quantities derived from OF estimation	Benz <i>et al.</i>	OF-based; Second-order div-curl regularization; Parameters: average, median, and maximum estimated intra-aneurysmal blood speed; Normalized by estimated speed in parent artery	[30]

represents a major conceptual paradigm shift in that not only the aneurysm itself is the target for treatment, but the diseased vessel segment as a whole. Flow diversion comprises the advantages of being an endovascular approach such as coil embolization, while at the same time reducing the need for placing material inside the aneurysm sac.<sup>1</sup> Especially in fusiform and giant wide-necked aneurysms, where endovascular coil embolization is complicated, flow diversion as an entirely endoluminal approach is thought to offer an effective and safe treatment option [12].

In spite of the attractive features of flow diversion therapy, it has one major limitation, which is inherent to its healing approach; immediately after treatment the aneurysm is still patent. It has been shown for many cases that FD deployment yields to the occlusion of aneurysms; however, there is no guarantee to this. Current interventional methods cannot sufficiently determine whether an aneurysm is going to be occluded. Hence, until the aneurysm eventually will undergo occlusion, there is—if low—remaining risk of hemorrhage.

This shortcoming of flow diversion gives rise to the clinical need for predicting treatment outcome during the intervention. Currently, the gold standard for deciding upon prospective treatment success is the visual evaluation of 2-D digital subtraction angiography (DSA) series. This highly subjective method is of limited use for the implementation of standard clinical guidelines. It is therefore of high clinical interest to develop methods that, based on DSA series, yield quantifiable indices that describe hemodynamic changes induced by flow diversion therapy.

This paper describes and proposes a novel algorithmic approach towards estimating the efficacy of FD treatments based on DSA series. The approach is based on assessing the level of pulsatility inside the aneurysm before and after FD treatment. To this end, a frequency analysis of signals derived from angiographic series is suggested. This allows quantifying the prevalence of frequency components in the aneurysm signal that correspond to the patient's heart rate.

<sup>1</sup>Some manufacturers, however, recommend to deploy their FDs in combination with intra-aneurysmal coils.

## II. RELATED WORK

In the past, several approaches towards the quantification of hemodynamics in cerebral aneurysms based on angiographic imagery have been proposed. In order to place the approach suggested in this paper into context, this section provides an extended overview of the state-of-the-art. A brief overview of the methods discussed in this section is given in Table I.

### A. The SMART Scale

Similar to the Raymond-Roy scale for endovascular coil embolization of cerebral aneurysms [31], Grunwald *et al.* proposed the SMART (simple measurement of aneurysm residual after treatment) scale for assessing flow diverter performance [13]. The SMART scale is a simple five-point grading scale specifically designed for the angiographic assessment of aneurysms treated by means of flow diversion. Primary diagnostic criteria for grading are inflow characteristics, amount of contrast agent stasis, and location of stasis. Grade 0, for instance, is assigned to any aneurysm with an early, coherent inflow jet, while grade 4 represents a completely occluded aneurysm. The SMART scale is suggested to be applicable to both saccular and fusiform aneurysms.

The major asset of the SMART scale lies in its simplicity. It can be applied easily without the need for additional technology. It incorporates visual criteria familiar to practitioners, that have additionally been reported to be of clinical significance (e.g., eclipse sign). Furthermore, it offers guidance in terms of cues to pay attention to and boils down several visual impressions into a single grade. With respect to subjectivity, the SMART scale certainly is an improvement over the mere visual assessment of the angiographic scene after FD deployment. Yet, it remains a semi-objective method. The grading may vary significantly between observers, making it difficult to truly assess the performance of such a grading scheme. Moreover, the SMART scale runs risk of oversimplifying the problem at hand. Subtle differences that cannot accurately be represented within the rather coarse grading scheme, may be of critical importance.

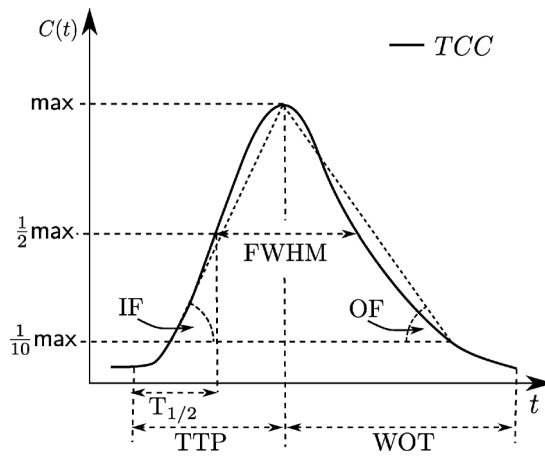


Fig. 1. Illustration of the curve parameters TTP,  $T_{1/2}$ , FWHM, IF, OF, and WOT.

### B. Methods Based on Time-Contrast Curve Analysis

A variety of metrics that have been proposed to angiographically assess hemodynamics in cerebral aneurysms are based on the analysis of time-contrast curves (TCC). A TCC is a discrete-valued time series obtained by extracting the average image intensity value over time within a region of interest (ROI) of a DSA series. Often, specific mathematical models are fitted to the raw TCC in order to yield a continuous curve. TCCs extracted from ROIs covering the inside of a cerebral aneurysm in DSA series acquired before and after FD treatment are commonly considered in order to assess hemodynamic modifications induced by FD deployment. To this end, curve parameters derived from each respective TCC can be investigated.

1) *Direct Evaluation of TCC Parameters:* All TCC-based methods described in this section use subsets of the same set of curve parameters. Commonly used parameters are, for instance, time to peak (TTP), time to half peak ( $T_{1/2}$ ), mean transit time (MTT), full-width at half-maximum (FWHM), average inflow (IF), average outflow (OF), and wash-out time (WOT) (cf. Fig. 1). While the curve parameters that were considered in the individual methods are roughly the same, they differ in their choice of model fitted to the raw TCC. Moreover, different normalization schemes were investigated and the selection of ROIs varied in between studies.

Tenjin *et al.* [14] investigated blood flow velocities in 31 cerebral aneurysms by means of TCCs extracted from DSA runs acquired at 30 frames per second (fps). In addition, velocity estimates were obtained in regions proximal and distal to the aneurysm on the parent artery. For this purpose, ROIs proximal and distal to the parent artery as well as on the aneurysm itself were selected. TTP,  $T_{1/2}$ , and MTT were used as curve parameters. For the calculation of TTP, the TCC was fitted to a gamma-variate function. In case of MTT, the TCC was numerically integrated and the MTT was defined as  $T_{1/2}$  of the integration curve. The results suggested that velocities inside smaller aneurysms are faster than inside larger aneurysms. There was no significant difference in MTT,  $T_{1/2}$ , and MTT of the TCCs from the ROIs on the parent artery and the aneurysm itself.

Asakura *et al.* [15] assessed the blood flow in cerebral aneurysms before and after they had undergone endovascular coil embolization. DSA sequences acquired at 6 fps were used and TCCs were extracted from ROIs inside the aneurysm. A two-exponential model that describes the change of contrast agent over time, during both the wash-in and wash-out phase of contrast, was fit to the time-contrast data points. The exponential-coefficient of the wash-in curve was then used as an estimate for intra-aneurysmal blood flow. A significant decrease of this parameter was found in small aneurysms treated with coil embolization.

Wang *et al.* [16], [17] aimed at documenting the effect of contrast settling in aneurysm domes by means of TCC parameters. The term contrast settling describes an effect that is presumably caused by gravity and the density difference between contrast agent and blood. In an *in vitro* study, one ROI was delineated on the proximal part (ROI-2) of the parent artery and one on the aneurysm sac (ROI-1). As curve parameters, the maximum value and WOT were used. The maximum value was calculated from a polynomial fit to the peak region and the WOT from an exponential fit to the trailing part of the curve. Both curve parameters seemed to be good indicators for contrast settling. Furthermore, Wang *et al.* attempted to minimize the variations of hand injection in the aneurysm TCC (ROI-1) by deconvolution with the inflow TCC (ROI-2).

Ionita *et al.* [18]–[20] presented a TDC-based method that is directly concerned with assessing intra-aneurysmal contrast flow modifications induced by FD treatment.<sup>2</sup> Novel asymmetric flow-diverting stents were placed across the neck of cerebral aneurysms created in animals. To obtain a normalized TDC (NTDC), the TDC extracted from each aneurysm was normalized by the total amount of contrast agent passing through the vessel segment and the contrast velocity, which was found by means of a bolus-tracking algorithm [32].

In one study [18], the maximum value of the NTDC was chosen as the only curve parameter. In addition, the ratio of maximum values before and after FD treatment was calculated. The obtained ratios of the maximum values of pre- and post-treatment NTDCs suggested a radical reduction in intra-aneurysmal contrast flow.

In another study [19], maximum value, TTP, MTT, IF, and WOT were investigated as curve parameters. Pre-post ratios were derived as well. The curve parameters were calculated from a linear fit to the rising part and an exponential fit to the trailing part of the NTDC. While all curve parameters indicated reduced aneurysmal flow after FD deployment, the correlation with the treatment outcome was more successful for curve parameters that were related to the contrast bolus injection (maximum value and IF) than for time-related parameters (WOT, MTT, TTP).

Struffert *et al.* [21] conducted an animal study where TCCs before and after endoluminal treatment were extracted from DSA series of elastase-induced aneurysms in rabbits. The treatment consisted of either the deployment of a conventional intracranial stent or an FD. A single ROI covering most of the inside of the aneurysm was delineated in each DSA series. The

<sup>2</sup>Ionita *et al.* preferred the term time-density curve (TDC) over the term TCC. Both terms refer to the same concept.

model chosen to obtain smooth TCCs was equal to the one presented by Sadasivan *et al.* [22]. TTP, FWHM, IF, and OF were selected as curve parameters. In addition, the obtained TCCs were also evaluated visually. TTP and FWHM were found to be significantly decreased after FD deployment. The effect on TTP and FWHM was less in case of treatment with a conventional stent. IF and OF were significantly reduced in aneurysms treated with an FD, while the reduction was less in conventionally stented aneurysms. Visually, a clear distinction between TCCs from before and after treatment could be made. Furthermore, practitioners were able to differentiate between TCCs extracted from aneurysms treated with a conventional stent and those treated with an FD.

In general, direct TCC parameters can be efficiently obtained and thus pose a feasible alternative to nonquantifiable criteria for FD treatment evaluation. Yet, their usefulness is uncertain since the body of published evidence is small and inconsistent. There is evidence suggesting that some simple parameters such as contrast stagnation which are accessible by direct evaluation of TCC parameters are not a good predictor for FD treatment success [29]. Most TCC-based methods neglect advanced properties of TCCs such as variability induced by the cardiac activity, which our approach focuses on (cf. Section III-A). Apart from parameter selection, choosing a suitable model to fit the TCCs is a challenge for methods that directly evaluate TCC parameters. The TCC-based methods described thus far employ models that were chosen empirically and lack physical justification.

2) *Washout Coefficient*: The washout coefficient proposed by Sadasivan *et al.* [22]–[27] is a TCC-based metric for assessing the performance of FD deployments. In contrast to other methods reviewed in this paper, the model that is fit to the TCC data points is justified by fluid dynamics considerations. In addition, several parameters are incorporated into a single index, called the washout coefficient, which is thought to serve as a predictor for treatment success. The parameters that are included in this coefficient are a subset of the best-fit parameters obtained from function fitting; i.e., none of the other standard curve parameters as described above (e.g., TTP, IF, etc.) are considered.

To calculate the washout coefficient, first a mathematical model is fit to a TCC extracted from an ROI covering the aneurysm sac

$$\begin{aligned} f(t) &= f_{\text{conv}}(t) + f_{\text{diff}}(t) \\ &= \rho_{\text{conv}} \int_0^t \frac{1}{\sigma\sqrt{2\pi}} e^{(\eta-\mu)^2/2\sigma^2} * \frac{1}{\tau_{\text{conv}}} e^{-((t-\eta)/\tau_{\text{conv}})} d\eta \\ &\quad + \rho_{\text{diff}} \left[ \int_0^t \frac{1}{\sigma\sqrt{2\pi}} e^{(\eta-\mu)^2/2\sigma^2} d\eta - (1 - e^{-(t/\tau_{\text{diff}})}) \right]. \end{aligned} \quad (1)$$

This mathematical model can be split into two parts, the convective component  $f_{\text{conv}}$  and the diffusive component  $f_{\text{diff}}$ . The two fluid dynamics processes, advection and diffusion, that govern the transport of contrast agent into and out of the aneurysm are thus what is being described by the two components of this model. The first part  $f_{\text{conv}}$  models contrast medium that enters and leaves the aneurysm by means of advection. Advection in this context means that contrast agent is carried

away by the bulk motion of the flowing blood. Mathematically,  $f_{\text{conv}}$  is expressed as a normal distribution convolved (\*) with an exponential decay. The second part  $f_{\text{diff}}$  models the diffusive transport component which is expressed as a sigmoid function and, again, an exponential decay. As an approximation to the integral of a normal distribution, the sigmoid function represents contrast medium that is advected into the aneurysm and trapped inside until it diffuses into outward flows.

The modelling follows the assumption that the proportions of advective and diffusive transport are reversed by the placement of an FD. Before FD treatment, contrast agent transport in and out of the aneurysm is assumed to be mainly governed by advection. In contrast, after FD deployment contrast agent transport is expected to be predominantly controlled by diffusion.

Six parameters have to be optimized in order to fit the model to the data.  $\mu$  and  $\eta$  apply to both the convective and diffusive component and are thus not useful for detecting proportional changes between the two parts. The other four parameters, however, can be employed for such a task. The parameters  $\rho_{\text{conv}}$  and  $\rho_{\text{diff}}$  represent the relative magnitudes of convective and diffusive transport, respectively. Before FD placement  $\rho_{\text{conv}} > \rho_{\text{diff}}$  and afterwards  $\rho_{\text{conv}} < \rho_{\text{diff}}$  is expected.  $\tau_{\text{conv}}$  and  $\tau_{\text{diff}}$  stand for the (absolute) time constants of the exponential decay in the convection and diffusion component, respectively. After FD treatment an increase in both, with a stronger increase in  $\tau_{\text{diff}}$ , is expected to be observed.

While the fitting of the fluid dynamics based model is far more central to this method than to the other TCC-based methods that have been presented here, it is still just a prerequisite for deriving the actual washout coefficient. The washout coefficient  $W$  is defined as [25]

$$W = \frac{\delta\% \cdot \rho_{\text{diff}}\% \cdot \tau_{\text{diff}}\%}{10^6} \quad (2)$$

where  $\delta$  represents the amplitude of the sum of the convective and diffusive components, and  $\rho_{\text{diff}}$  and  $\tau_{\text{diff}}$  are the relative magnitude and time constant of the diffusive component, respectively. All quantities are obtained post-treatment and the % sign indicates that they are expressed as percent ratios to the respective values before treatment. In some studies, the aforementioned mathematical model was fit to TCC data but the actual washout coefficient was not computed. Instead, the best-fit parameters and their ratios before and after treatment were compared directly [22], [26].

The best-fit parameters of the model have been proven to correlate well with PIV measurements [24]. In an animal study, the predictive value of the washout coefficient was assessed [23]. It was suggested, that  $W < 30$  predicts a probability greater than 97% of complete aneurysm occlusion after six months (SE 73%, SP 82%).

The fluid mechanical justification is what sets apart this approach from other TCC-based methods. The definition of the washout coefficient, however, is problematic since it leads to inconsistencies, which, for instance, make this metric inapplicable to control aneurysms. For an untreated control aneurysm, the washout-coefficient is equal to one ( $W = 1$ ). On the other hand, it was suggested that  $W < 30$  predicts a high rate of aneurysm occlusion. An untreated aneurysm is highly unlikely

to belong to the cohort of aneurysms that have successfully been occluded, therefore  $W < 30$  cannot be a reliable predictor for aneurysms with  $W \approx 1$ .

3) *Intra-Aneurysmal Flow to Arterial Flow Ratio*: Jou *et al.* [28] recently proposed a technique which attempts to assess the ratio of the intra-aneurysmal flow to the flow rate in the parent artery. The technique is based on the analysis of DSA series as well as a volume reconstruction of the diseased vessel segment obtained from a 3-D rotational angiography (3DRA) run. Two ROIs, one proximal and one distal to the aneurysm neck, were selected (ROIs  $i$  and  $o$ ). Optionally, a third ROI covering the inside of the aneurysm was delineated (ROI  $a$ ). To determine the associated volumes of the ROIs, they were projected back onto the vessel volume obtained from the 3-D reconstruction. For each ROI, a TCC  $c_{ROI}$  was extracted and normalized by the ROI volume. The signals obtained in this manner for the proximal ( $c_i$ ), distal ( $c_o$ ), and aneurysm ( $c_a$ ) ROI were assumed to be proportional to the concentration of contrast agent in the respective ROI.

Subsequently, the balance of contrast medium could be stated as

$$Q_i c_i - Q_o c_o + \alpha Q_a c_a = Q_i c_o \quad (3)$$

where  $Q_i$ ,  $Q_o$ , and  $Q_a$  represent the flow rates in each of the ROIs  $i$ ,  $o$ , and  $a$ , respectively. The parameter  $\alpha$  renders the concentration of contrast agent leaving the aneurysm proportionally dependent on the concentration of contrast agent inside the aneurysm ( $c_a$ ). Subsequently, the intra-aneurysmal flow ratio  $f$  was defined as the ratio of the intra-aneurysmal flow to the flow rate in the parent artery

$$f = \frac{Q_a}{Q_i}. \quad (4)$$

Through further intermediate mathematical steps, this  $f$ -number was derived for seven unruptured cerebral aneurysms and compared to the same ratio obtained from CFD simulations. The correlation was reported to be very good in case of 30 fps DSA series and worse when conducting the same experiment with a downsampled version of the series (15 and 7.5 fps).

It was suggested, that a high  $f$  implies a larger intra-aneurysmal flow ratio and often represents a system where the plots of  $c_i$  and  $c_o$  are likely to not resemble each other in appearance. Furthermore, in cases of  $f$  being high,  $c_a$  was reported to exhibit a stronger cardiac variation, thereby resembling the inflow curve  $c_i$ . In contrast, a smaller  $f$  would imply a smaller intra-aneurysmal flow ratio and  $c_i$  and  $c_o$  curves that look alike. Beat-to-beat variation of  $c_a$  was reported to be less in cases of a smaller  $f$ , which indicates a decoupling of the aneurysmal flow from the flow in the parent artery.

Jou *et al.* went beyond the direct assessment of curve parameters by considering the beat-to-beat variation in the derived signals. Our methodology adopted this idea since it potentially provides more insight into hemodynamic modifications induced by FD treatment. A drawback of the technique proposed by Jou *et al.* is that a volume reconstruction obtained from a 3-D DSA run is a prerequisite for deriving the metric, which adds time and effort to the workflow.

### C. Methods Based on Optical Flow Estimation

The dynamic behavior of contrast agent in a DSA series can be assumed to be closely coupled to the flow of blood in the observed vasculature. To quantify blood flow based on DSA series, it seems thus appropriate to estimate contrast agent motion in the respective vessel segment. Obviously, spatial resolution constraints prohibit the tracking of individual particles. Given a modest injection rate, however, the contrast medium diluted in the bloodstream exhibits local brightness patterns whose apparent motions can be estimated by means of specific optical flow (OF) algorithms. This perceived motion can be regarded as being dependent on the actual 3-D flow of blood. Therefore, estimating 2-D velocity fields by means of OF algorithms can be used to gain insight into blood flow conditions in the diseased vessel segment.

OF estimators aim at recovering the perceived 2-D motion of image features in a scene by computing a displacement field  $\vec{u} = (u_1, u_2)^T$  of corresponding pixels from at least two subsequent images  $I(\vec{x}, t)$  and  $I(\vec{x}, t + 1)$  of the scene. The classic 2-D OF constraint assumes constant brightness of two corresponding pixels; i.e.,

$$I(\vec{x}, t) = I(\vec{x} + \vec{u}, t + 1). \quad (5)$$

By linearization through a first-order Taylor series expansion of the right-hand side of (5), we arrive at

$$I_t + \nabla I \cdot \vec{u} = 0 \quad (6)$$

where  $\nabla I = (I_x, I_y)$  and  $I_{\bullet} = \partial I / \partial \bullet$ . In case of image sequences comprising well-defined objects and salient features, the brightness constancy assumption is reasonable. In the context of recovering OF from transmittance imagery of fluid flow (e.g., DSA series), however, brightness constancy is easily violated. It was thus suggested to replace the OF data term [(6)] by a more physically justified constraint based on conservation of mass [33], [34]. The amount of attenuation of a fluid such as blood is generally related to the density of a physical quantity dispersed in the fluid. In case of DSA series, the density of contrast agent particles represents this quantity. The contrast agent is advected by the blood flow, a transport process that respects the conservation of mass constraint. Thus, the continuity equation can be set up for the density  $\rho$  of contrast agent

$$\frac{\partial \rho}{\partial t} + \nabla \cdot (\rho \vec{v}) = 0 \quad (7)$$

where  $\nabla \cdot$  is the divergence operator and  $\vec{v}$  is the 3-D velocity field. The continuity equation in this form simply states that the temporal change in density is equal to the flux of density through the boundary of an infinitesimal volume. For image formation processes similar to X-ray imaging, it can be shown [33] that the continuity equation is still satisfied in 2-D, when replacing the density  $\rho$  with the image intensity  $I$

$$I_t + \nabla \cdot (I \vec{u}) = 0 \quad (8)$$

with  $\vec{u}$  being the density-weighted average along an imaging ray and assuming no normal flow out of the specimen [35]. In contrast to (6), (8) represents a physically justified data term that

is possibly more suitable for recovering fluid flow from angiographic imagery.

For each pixel, (8) needs to be solved for two unknown variables ( $u_1$  and  $u_2$ ), rendering it ill-posed. In order to obtain a well-posed problem, additional constraints need to be considered. Typically, spatial coherence is assumed, meaning that neighboring pixels share the same velocity. This implies a smoothly varying motion field estimate. Regularization in variational optimization schemes is often conducted by searching for solutions that minimize the energy functional

$$\int_{\Omega} \|\nabla u_1\|^2 + \|\nabla u_2\|^2 dx dy \quad (9)$$

on the image domain  $\Omega$ . It can be shown [36] that the minimization of (9) is equivalent to the minimization of

$$\int_{\Omega} \operatorname{div}(\vec{u})^2 + \operatorname{curl}(\vec{u})^2 dx dy \quad (10)$$

a first-order div-curl regularizer. Therefore, OF estimators that minimize (9) (e.g., [34]) penalize nonlaminar flow, where  $\operatorname{div}(\vec{u}) \neq 0$  and  $\operatorname{curl}(\vec{u}) \neq 0$ .

The mean aneurysm flow amplitude (MAFA) index introduced by Pereira *et al.* [29] is a related OF-based technique. To derive the MAFA index, the time-averaged estimated velocity in an ROI covering the aneurysm sac is first computed. An OF estimator similar to [34] is employed for this purpose. To assess differences induced by FD placement, the MAFA ratio  $R$  is then defined as

$$R = \frac{\operatorname{MAFA}_{\text{post}}}{\operatorname{MAFA}_{\text{pre}}} \cdot \frac{Q_{\text{pre}}}{Q_{\text{post}}} \quad (11)$$

where  $\operatorname{MAFA}_{\text{pre}}$  and  $\operatorname{MAFA}_{\text{post}}$  are the time-averaged estimated velocities from DSA series acquired before (pre) and after (post) treatment.  $Q_{\text{pre}}$  and  $Q_{\text{post}}$  represent the estimated volumetric flow in the parent artery estimated before and after FD placement, respectively.  $Q$  is determined by obtaining the cross-sectional area in an ROI on the parent artery from a 3-D reconstruction of the vessel and combining this information with velocity estimates from OF computations inside this ROI.

It was attempted to compute the MAFA ratio based on 24 DSA runs (60 fps) before and after treatment. To assess the predictive value of the MAFA ratio, the computed values were correlated with the clinical outcome at follow-up. Pereira *et al.* concluded that the optimum threshold for the MAFA ratio to predict aneurysm occlusion at 12 months was 0.96 ( $p = 0.009$ , ACC 90%) for those cases where flow parameters could be obtained.

In the case of fluid flow, where regions with highly nonlaminar flows can be as prevalent as regions with laminar flows, a first-order regularizer that penalizes nonlaminar flow can be disadvantageous. To this end, Corpetti *et al.* [37] proposed the use of a second-order div-curl regularizer [38]

$$\int_{\Omega} \|\nabla \operatorname{div}(\vec{u})\|^2 + \|\nabla \operatorname{curl}(\vec{u})\|^2 dx dy \quad (12)$$

in addition to using the data term given in (8). This regularizer promotes smoothly varying divergence and curl fields instead of penalizing nonlaminar flow estimates.

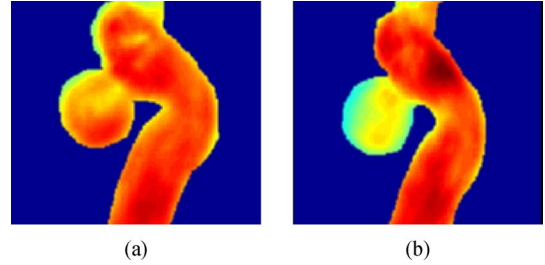


Fig. 2. Time-averaged estimated velocity magnitude of one aneurysm case [30]; (a) before FD treatment, (b) after FD treatment. A clear reduction in the average velocity can be observed immediately after treatment with a flow-diverting stent. Please refer to the electronic version of this article for color indication.

Our group recently proposed an OF-based approach for the angiographic analysis of FD efficacy [30]. Following [37], an OF estimator designed for recovering fluid flows was employed since it was assumed to be advantageous in case of turbulent flows. Apart from the time-averaged velocity in aneurysm ROIs, several other metrics derived from the estimated flow fields were studied. Normalization with respect to incoming blood flow was conducted by estimating flow in an ROI covering parts of the parent artery, proximal to the aneurysm. In this setting, a 3DRA acquisition was not a prerequisite, a factor that could benefit integration into clinical workflow. Initial results yielded by a feasibility study on 34 DSA series were encouraging. Fig. 2 gives a visual impression of one of the results obtained.

Approaches that employ OF estimation for FD treatment evaluation are appealing since they aim at directly recovering parameters of the projected blood flow field. The main drawback is the computational effort involved in recovering flow field estimates, which is an inherently ill-posed problem requiring complex regularization, unobstructed views and high DSA frame rates (up to 60 fps are used in [29]). Computation of the MAFA ratio requires a 3-D volume reconstruction from a 3-D DSA run that needs to be acquired in addition to the pre- and post-treatment DSA runs, thereby adding time and effort to the workflow.

### III. THEORY AND METHODS

#### A. Conceptual Basis

In a typical clinical setting, oscillating patterns modulated on top of the general outline of TCCs can often be observed. These modulations of the TCCs are mostly caused by the cardiac cycle. During the contraction of the heart (systole), the amount of blood entering the vessel segment of interest increases. Thus, given a constant rate of contrast agent injection, the net contrast agent concentration decreases. Therefore, during systole, the TCC declines and assumes a local minimum. The opposite is true during diastole, the relaxation of the heart. Here, the contrast agent concentration in blood increases and thus the TCC rises and reaches a local maximum. Fig. 3 shows an illustration of a TCC that exhibits such a beat-to-beat variation. Besides a reasonably selected frame rate, the modulations due to the cardiac cycle are only visible if the contrast agent concentration is

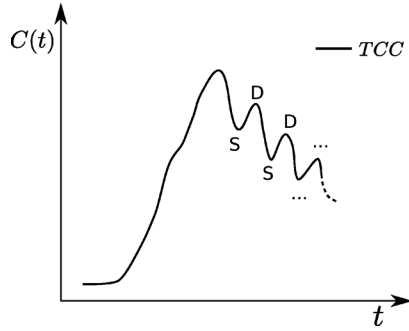


Fig. 3. This illustration of a TCC exhibits an oscillating pattern induced by the cardiac cycle. During systole (S), the net contrast agent concentration decreases; during diastole (D), it increases.

sufficiently low and the injection duration suitably long. Otherwise, the modulations are prone to be hidden by saturation effects.

Soon after the advent of DSA, attempts were made to extract information from such beat-to-beat variations [39]. Quantifying by how much a TCC corresponding to an ROI placed on top of a cerebral aneurysm fluctuates with each cardiac cycle, has, to our knowledge, not been studied before. Such quantification could be beneficial when assessing the efficacy of FD deployments. When deriving a parameter that does not depend on the absolute contrast medium concentration, the relative amount of blood entering the aneurysm during each cardiac cycle could be studied. A decrease in relative blood volume entering the aneurysm after FD deployment compared to the same quantity before treatment could be regarded favorably for inducing thrombus formation. If, in addition, the amount of beat-to-beat variation in the parent artery is incorporated into this parameter as a normalization factor, it could be considered a quantity that detects the amount of coupling of the aneurysm to the parent artery. A decrease of the parameter derived from a TCC placed on top of an aneurysm relative to the same quantity derived from a TCC of an ROI on the parent artery, could then indicate a decoupling of the aneurysm from the healthy circulation of blood.

In this paper, a metric is proposed that aims at capturing the change in beat-to-beat variations between two TCCs extracted from an ROI covering the same anatomy, but at different points in time. The metric is retrospectively applied to pairs of DSA series of cerebral aneurysms, whereby one DSA series was acquired before and the other was acquired after FD treatment. It is suggested that this metric can offer predictive value with respect to determining clinical outcomes of cerebral aneurysms treated with FDs.

When seeking to assess the variation induced by the cardiac cycle, one can compute the difference between the end-diastolic value (EDV) and the end-systolic value (ESV) of the TCC. The EDV is the value that the TCC attains right before a contraction of the heart (local maximum of the TCC), while the ESV is the value that the TCC attains right after a contraction of the heart (local minimum of the TCC). When trying to compare this difference obtained from two different TCCs, one needs to scale the quantity with respect to some base-level. Given a constant volume, the absolute difference between EDV and ESV

depends on both the volumetric difference and the total contrast agent concentration in the volume. Therefore, relative differences instead of absolute differences should be used in comparative studies.

To compute the difference between EDV and ESV, it is possible to extract both of them from a TCC and subtract them. In order to get a better estimate, the average value of the differences at a number of different heart cycles can be computed [39]. From a signal processing point of view, this problem can be approached by considering the representation of the TCC in frequency domain. When thinking about the TCC as a composition of sinusoids, we may consider the difference between EDV and ESV as the amplitude of the sinusoidal component that has a frequency equal to the heart rate. In other words, a TCC that exhibits a pulsatile pattern is expected to have a high amount of energy in its power spectral density (PSD) [40] at a frequency corresponding to the heart rate. We therefore suggest to quantify pulsatile variations of a TCC induced by the cardiac cycle by estimating its PSD and subsequently averaging the power over a range of frequencies around the heart rate. To assess the change in the amount of pulsatility, the amount of energy at frequencies around the heart rate is compared between TCCs extracted from ROIs covering the inside of an aneurysm before and after FD treatment. Fig. 4 outlines this process.

### B. Pulsatility Ratio

For estimating the PSD of a TCC, the periodogram estimator was used [40], which is a PSD estimator based on the discrete Fourier transform (DFT). The pulsatility  $\mathbf{P}$  of a TCC with respect to a certain frequency range was defined as the average of the periodogram at frequencies within this range

$$\mathbf{P}_{\text{TCC}}(f_l, f_h) = \frac{\sum_{k=\lfloor (f_l/\Delta f) + (1/2) \rfloor}^{\lfloor (f_h/\Delta f) + (1/2) \rfloor} \hat{\Phi}_P(f_k)}{\lfloor (f_h/\Delta f) + (1/2) \rfloor - \lfloor (f_l/\Delta f) + (1/2) \rfloor + 1} \quad (13)$$

where  $f_l$  and  $f_h$  are the lower and higher bounds of the frequency range, respectively,  $\Delta f$  the bin width of the DFT ( $\Delta f = F_s/N$ , where  $F_s$  is the sampling frequency and  $N$  the number of samples),  $f_k = k\Delta f$ , and  $\hat{\Phi}_P$  the periodogram estimator of the TCC (as, for example, defined in [40])

$$\hat{\Phi}_P(f) = \frac{1}{N} \left| \sum_{n=1}^N \text{TCC}_n e^{-2\pi i f n} \right|^2. \quad (14)$$

Furthermore, the pulsatility ratio  $\mathbf{PR}$  was defined as the reciprocal ratio of the pulsatility  $\mathbf{P}$  before ( $\mathbf{P}^{\text{pre}}$ ) and after ( $\mathbf{P}^{\text{post}}$ ) FD deployment

$$\mathbf{PR}_{\text{TCC}} = \frac{\mathbf{P}_{\text{TCC}}^{\text{post}}}{\mathbf{P}_{\text{TCC}}^{\text{pre}}} \quad (15)$$

which means that  $\mathbf{PR} < 1$  indicated a decrease in pulsatility after treatment. The frequencies  $f_l$  and  $f_h$  have been omitted in (15). In our experiments, they have been chosen to be the same in  $\mathbf{P}^{\text{pre}}$  and  $\mathbf{P}^{\text{post}}$ . In general, however, they are allowed to change to account for, for instance, a change in the patient's heart rate.

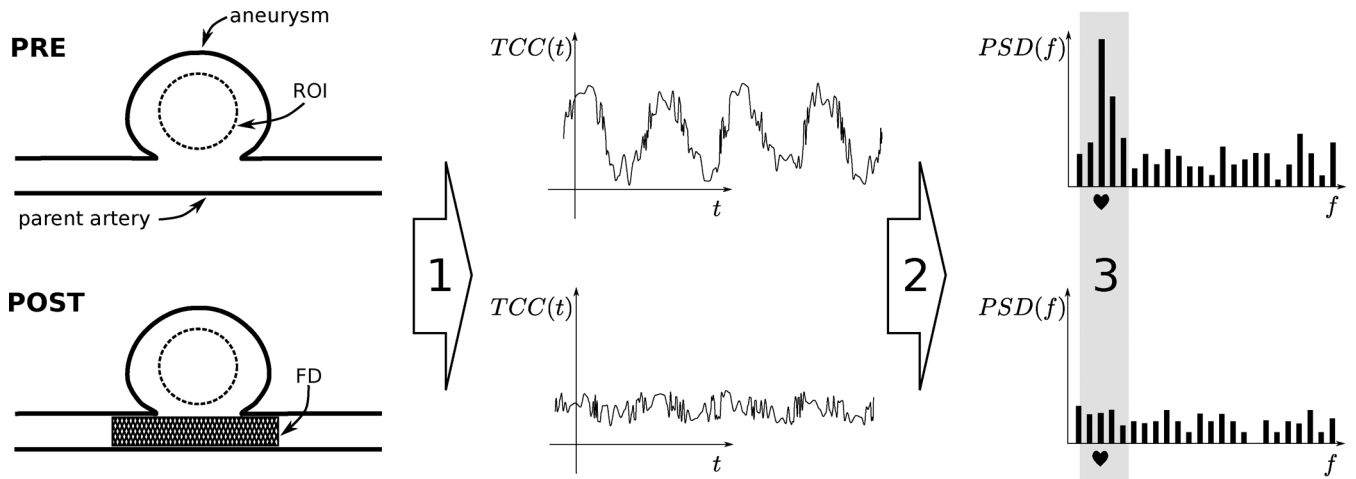


Fig. 4. Two ROIs are delineated in DSA series acquired before and after treatment. TCCs are extracted from both ROIs and preprocessed (1). PSD is estimated for both TCCs (2). PSD estimates are compared with respect to a certain frequency range around the heart rate (3). The same process can be repeated for ROIs in the parent artery, proximal to the aneurysm (not shown). This proximal ratio can then be incorporated into the comparison as a normalization factor.

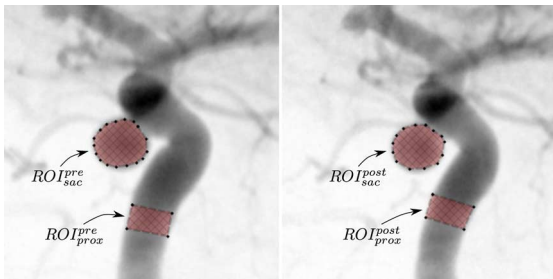


Fig. 5. Exemplary selection of ROIs in DSA series acquired before (left) and after (right) FD deployment.  $ROI_{sac}^{pre}$  covers the inside of the aneurysm and  $ROI_{prox}^{pre}$  covers parts of the parent artery proximal to the aneurysm. Both images represent maximum opacification plots of the respective series.

To compute the  $PR$  of a TCC extracted from an ROI covering the inside of an aneurysm ( $PR_{sac}$ ), ROIs in the aneurysm were selected in DSA series acquired before and after FD deployment ( $ROI_{sac}^{pre}$  and  $ROI_{sac}^{post}$ ). Optionally, ROIs on the parent artery proximal to the aneurysm were selected in both series ( $ROI_{prox}^{pre}$  and  $ROI_{prox}^{post}$ ). Fig. 5 shows an example of how those ROIs were selected.

Subsequently, the  $PR$  of TCCs extracted from  $ROI_{sac}^{pre}$  and  $ROI_{sac}^{post}$  was computed

$$PR_{sac} = \frac{P_{sac}^{post}}{P_{sac}^{pre}}. \quad (16)$$

In the same manner, the  $PR$  of TCCs extracted from  $ROI_{prox}^{pre}$  and  $ROI_{prox}^{post}$  was computed

$$PR_{prox} = \frac{P_{prox}^{post}}{P_{prox}^{pre}}. \quad (17)$$

By combining (16) and (17), the inflow-normalized pulsatility ratio,  $PR_{sac}^{norm}$ , was defined as the product of  $PR_{sac}$  and  $(PR_{prox})^{-1}$

$$\begin{aligned} PR_{sac}^{norm} &= PR_{sac} \cdot (PR_{prox})^{-1} \\ &= \frac{P_{sac}^{post}}{P_{sac}^{pre}} \cdot \frac{P_{prox}^{pre}}{P_{prox}^{post}}. \end{aligned} \quad (18)$$

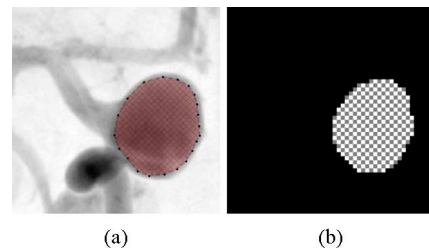


Fig. 6. (a) ROI covering the inside of an aneurysm is shown. (b) Rasterization of the ROI shown in (a). Neighborhood size is  $5 \times 5$  pixels and the minimum number of pixels in each neighborhood is 25 (only full rectangles).

If, for instance,  $PR_{sac} = PR_{prox} = 0.5$ ,  $PR_{sac}^{norm}$  would equate to 1 (no net change).

In the standard case, the TCC of an ROI was computed as the average of the TCCs of all pixels contained in the ROI. This practice corresponds to the coherent averaging of multiple DFTs in frequency domain. Due to the linearity of the DFT, the computation of just one DFT is necessary after having averaged the pixel-individual TCCs.

While being computationally efficient, this approach can be problematic since it assumes that the individual TCCs have constant phase [41]. To ease this assumption while still maintaining the benefits of spatial averaging, a method based on the averaging of several periodograms derived from the same ROI is proposed as well. In this method an ROI was decomposed into several small neighborhoods. Fig. 6(b) shows an example of such a rasterization. For each of the neighborhoods a periodogram was computed by averaging the TCCs of each pixel in the respective neighborhood. The periodogram of the entire ROI was then defined as the average of the periodograms of the neighborhoods. A checkerboard pattern was used to partition an ROI into multiple square neighborhoods of the same size. To avoid neighborhoods consisting of very few pixels, a threshold for the minimum number of pixels in a neighborhood was incorporated.

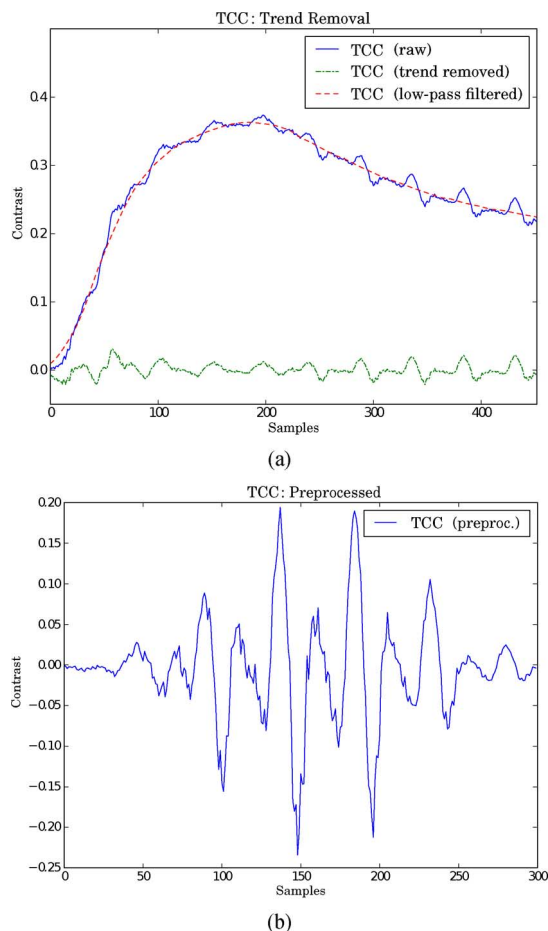


Fig. 7. Illustration of the preprocessing steps conducted for all TCCs. (a) Raw TCC (solid line), low-pass filtered TCC (dashed line), and TCC after trend-removal (dash-dotted line). (b) Same TCC as in (a) after Hamming windowing and inflow correction.

### C. Preprocessing

In order to avoid substantial leakage of very low frequency components into higher frequency components, the obvious overall trend (the wash-in and wash-out of contrast agent) was removed from the TCC. This was done by low-pass filtering the TCC in time domain and subtracting the filtered TCC from the original TCC. For this purpose, a moving average filter with a window size of  $2F_s$  was used. The signal boundaries were padded by constant replication of the respective boundary value on either side of the signal. Fig. 7(a) illustrates this preprocessing step using an example of a raw TCC and its low-pass filtered counterpart.

With this method, the large slope during the inflow of contrast agent seemed to cause artifacts in the amplitudes of the beat-to-beat variations. Therefore, the rising part of the TCC was cut off.

In order to remove the dependency of the amplitude of the beat-to-beat variations on the total contrast agent concentration in the ROI, the resulting curve was divided by the mean value of the original TCC.

The last step in preprocessing the TCC was data windowing by means of a Hamming window (a window coefficient of  $\alpha = 0.54$  was chosen empirically). The periodogram method was

TABLE II  
LOCATION, TYPE, AND SIZE (height  $\times$  width) OF THE ANEURYSM CASES UNDER INVESTIGATION

Case	Location	Type	Size (mm)
A1	Basilar tip	oval, irregular, intermediate neck	7 $\times$ 19
A2	ICA, para ophthalmic	berry, regular, small neck	8 $\times$ 8
A3	ICA, bifurcation	oval, irregular, very wide neck	8 $\times$ 6
A4	Basilar tip	berry, regular, small neck	7 $\times$ 5
A5	ICA, para ophthalmic	berry, regular, wide neck	16 $\times$ 16
A6	ICA, para ophthalmic	berry, regular, wide neck	24 $\times$ 16
A7	ICA, bifurcation	berry, regular, wide neck	13 $\times$ 12
A8	PComA	oval, irregular, wide neck	12 $\times$ 7
A9	ICA, choroidal	berry, regular, wide neck	7 $\times$ 6
A10	PComA	berry, regular, intermediate neck	5 $\times$ 3
A11	PComA	berry, regular, intermediate neck	4 $\times$ 3
A12	Basilar tip	berry, regular, wide neck	9 $\times$ 9
A13	ICA, para ophthalmic	berry, regular, wide neck	5 $\times$ 5

used to estimate the PSD of the preprocessed TCC. Fig. 7(b) gives an example of a fully preprocessed TCC.

For the subsequent Fourier analysis, all signals were zero-padded in order to yield a signal length equal to a power of two.

### D. Experimental Setup

In a first experiment,  $\mathbf{PR}_{\text{sac}}$  and  $\mathbf{PR}_{\text{sac}}^{\text{norm}}$  were calculated from 13 pairs of DSA series of cerebral aneurysms. In each case, one DSA series was acquired before and one after FD treatment. Contrast agent was delivered using a power injector (5 mL/s over 2 s at 300 pci pressure for a total of 10 mL, no dilution, 300:100 standard opaque material), X-ray delay was 1–1.3 s. While the amount of contrast was not as small as suggested by Jou *et al.* [28], the extracted TCCs still exhibited significant pulsatile variability [cf. Fig. 7(a)]. In some cases, cardiac variability patterns were more prevalent during the washout phase. This could be attributed to a contrast saturation effect as described by Ford *et al.* [42] in which pulsatile flow needs a short period of time to redevelop after contrast injection.

For this initial pilot study, we deliberately chose to apply the proposed metric on a rather diverse set of cerebral aneurysms, also featuring cases that were assumed to be challenging for the methodology. The aneurysms varied in size (small to giant) and shape (saccular, bifurcation). Table II provides an overview of the DSA series under investigation. DSA series of aneurysms in which vascular structures were superimposed on the aneurysm sac were included in the data set as well as cases where endovascular devices were visible. The frame rate of the DSA series was either 30 (A1) or 15 fps (A2–A13). Series A10 and A11 belonged to the same biplane DSA run. ROIs on the aneurysm and on the parent artery proximal to the aneurysm were delineated manually in a maximum opacification plot of each DSA series (cf. Fig. 5). The selection of ROIs was conducted regardless of superimposed vessels. It was attempted to delineate approximately the same ROIs in each pre- and post-treatment pair of DSA sequences. Since the study was conducted retrospectively, the heart rate during the DSA acquisitions was not accessible and thus assumed to be unknown. To cover a broad range of heart rates,  $f_l = 0.5$  Hz and  $f_h = 2.5$  Hz were thus chosen [cf. (15)]. In a real setting,  $f_l$  and  $f_h$  would be adjusted to the patient's heart rate (cf. Section III-B). With  $f_h = 2.5$  Hz, a frame rate of 15 fps adequately satisfies the Shannon sampling theorem up to the third harmonic (7.5 Hz), while a frame rate

TABLE III  
PULSATILITY RATIOS EXTRACTED FROM RASTERIZED  
AND UNRASTERIZED ROIS

Case	Unrasterized			Rasterized		
	$PR_{sac}$	$PR_{prox}$	$PR_{sac}^{norm}$	$PR_{sac}$	$PR_{prox}$	$PR_{sac}^{norm}$
A1	0.22	0.13	1.74	0.53	0.69	0.76
A2	2.06	0.85	2.43	0.72	0.56	1.28
A3	0.52	0.90	0.58	1.87	1.99	0.94
A4	3.01	0.67	4.51	1.08	3.01	0.36
A5	1.50	0.04	34.06	0.84	0.66	1.27
A6	8.01	0.25	31.68	0.06	0.48	0.12
A7	1.91	1.18	1.62	0.95	0.36	2.67
A8	0.79	1.66	0.48	0.98	1.02	0.97
A9	0.31	0.29	1.06	0.43	0.47	0.92
A10	0.25	0.48	0.51	0.31	0.61	0.51
A11	0.18	0.79	0.23	0.46	1.44	0.32
A12	.002	0.01	0.20	0.34	0.73	0.46
A13	0.12	1.65	0.07	0.35	0.92	0.38
AVG	1.45	0.69	6.09	0.68	0.99	0.84
MD	0.52	0.67	1.06	0.53	0.69	0.76
SD	2.10	0.54	11.49	0.45	0.72	0.64

of 30 fps is able to catch up to the sixth harmonic. On average, however, we expect a patient's heart rate to be well below 2.5 Hz. Assuming a heart rate of 90 bpm (1.5 Hz), for instance, a sampling rate of 15 fps would allow a capturing of up to the 5th harmonic, 30 fps even of up to the tenth harmonic. TCCs were extracted by means of averaging the TCC of each individual pixel within an ROI. The preprocessing of TCCs was conducted in the same manner as described above.

In a second experiment, the same methodology as in the first experiment was applied to the same set of DSA series, except that the ROIs were rasterized as described above and illustrated in Fig. 6. A neighborhood size of  $5 \times 5$  pixels and a minimum number of 25 pixels in each neighborhood was chosen during rasterization with a checkerboard pattern. The periodogram computation for the whole ROI was carried out in the same way as described in the experiment above.

In summary, the two experiments yielded, respectively, for each case A1-A13, the quantities  $PR_{sac}$ ,  $PR_{prox}$ , and  $PR_{sac}^{norm}$ ; once derived from unrasterized and once from rasterized ROIs.

#### IV. RESULTS AND DISCUSSION

##### A. Results

The pulsatility ratio  $PR_{sac}$  and the normalized pulsatility ratio  $PR_{sac}^{norm}$  were successfully calculated based on ROIs selected in 13 pairs of DSA series of cerebral aneurysms, each acquired before and after FD treatment. The quantities  $PR_{sac}$ ,  $PR_{prox}$ , and  $PR_{sac}^{norm}$  that were derived from the pulsatility  $P$  in the aneurysm and parent artery before and after FD deployment are given in Table III. A comparison of  $PR_{sac}$  and  $PR_{sac}^{norm}$  can be visually assessed in Fig. 8(a). The average value of  $PR_{sac}$  was 1.45, the median 0.52 (SD 2.10). In case of  $PR_{sac}^{norm}$ , the average was 6.09 and the median 1.06 (SD 11.49). The large standard deviations and differences between the mean and median are mainly due to A5 and A6. In both cases,  $PR_{sac}^{norm}$  are an order of magnitude higher than in the other cases. When omitting cases A5 and A6 from the statistical

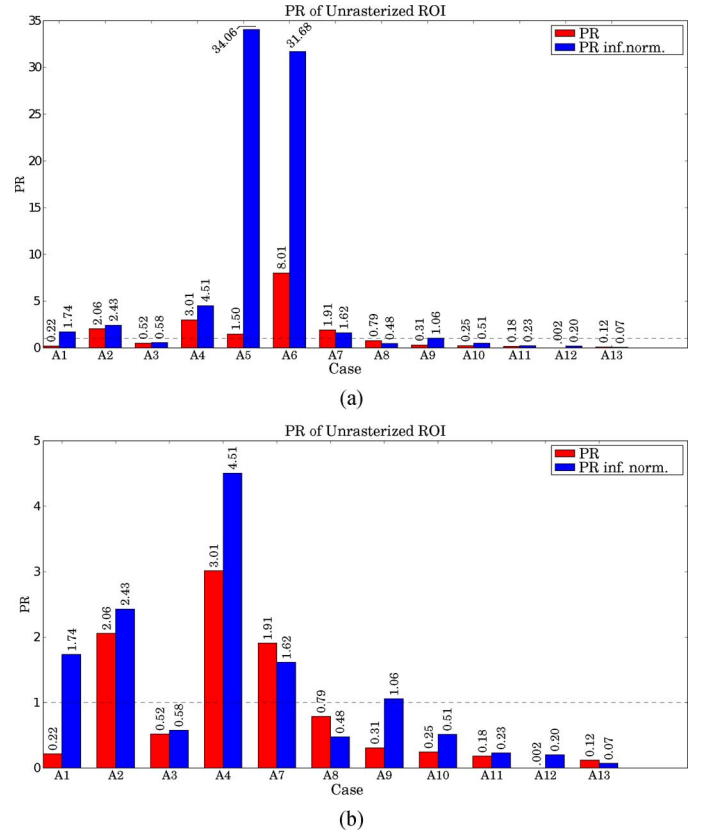


Fig. 8. Bar plots of  $PR_{sac}$  (red) and  $PR_{sac}^{norm}$  (blue). A value above 1 (dashed line) corresponds to an increase in pulsatility after FD deployment while a value below 1 corresponds to a decrease. Please refer to the electronic version of this article for color figures. (a)  $PR_{sac}$  (red) and  $PR_{sac}^{norm}$  (blue) for all 13 pairs of DSA series (A1-A13). Same plot without the outliers A5 and A6 is depicted in Fig. 8(b). (b) Same as Fig. 8(a), but without cases A5 and A6.

evaluation, the mean of  $PR_{sac}$  was 0.85, median 0.31 (SD 0.96), and the mean value of  $PR_{sac}^{norm}$  was 1.22, median 0.58 (SD 1.26). Still, the average values are influenced by case A4, which could also be regarded as an outlier. Overall, however, the results indicate a decrease of pulsatility in the aneurysm after FD treatment.

In the same manner as Fig. 8(a), Fig. 8(b) shows a comparison of  $PR_{sac}$  and  $PR_{sac}^{norm}$ , but without cases A5 and A6. Fig. 9 shows maximum opacification images of DSA series corresponding to A5 and A6. The parent vessel and several other vascular structures are superimposed onto the aneurysm in case of A5. A6 refers to a giant aneurysm which represented the largest aneurysm considered in this experiment.

The cases A10 and A11 are based on the same biplane DSA run and both exhibit decreased pulsatility after FD treatment. While sharing this same trend, the derived ratios are different from each other:  $PR_{sac}$  was 0.25 for case A10 (0.18 for case A11) and  $PR_{sac}^{norm}$  was 0.51 (0.23).

Fig. 10 depicts images of DSA series corresponding to the cases A1, A4, and A7. In all three cases, endovascular instruments seem to cause artifacts in the DSA acquisitions. In case of A1, an endovascular device can be seen in the parent artery, while in A4 and A7, a catheter seems to protrude into the inside of the aneurysm. Cases A1, A4, and A7 all belong to a group of

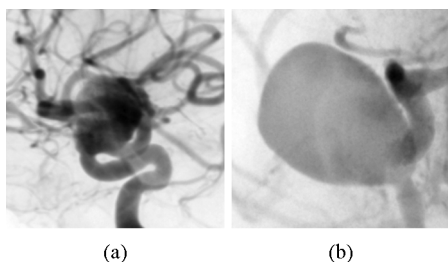


Fig. 9. Maximum opacification images of cases A5 (a) and A6 (b) are shown. Case A5 is a DSA run of a large aneurysm acquired with an unfavorable angulation. Parent artery as well as other opacified structures are superimposed onto several image regions inside the aneurysm. Case 6 is a giant aneurysm (the largest in the cohort used for the experiment). Both images shown are of size  $256 \times 256$  pixels.

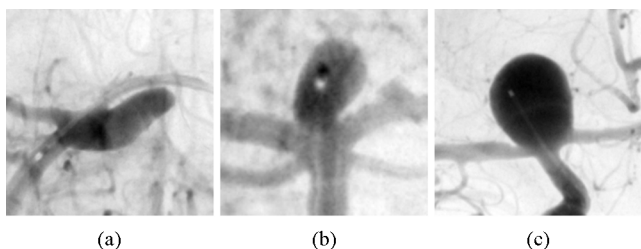


Fig. 10. Maximum opacification images of cases (a) A1, (b) A4, and (c) A7. Image artifacts due to endovascular devices can be seen in all three series (in the parent artery in case A1 and inside the aneurysm in cases A4 and A7). Images shown in (a) and (c) are  $256 \times 256$  each while the image in (b) is  $128 \times 128$  pixels.

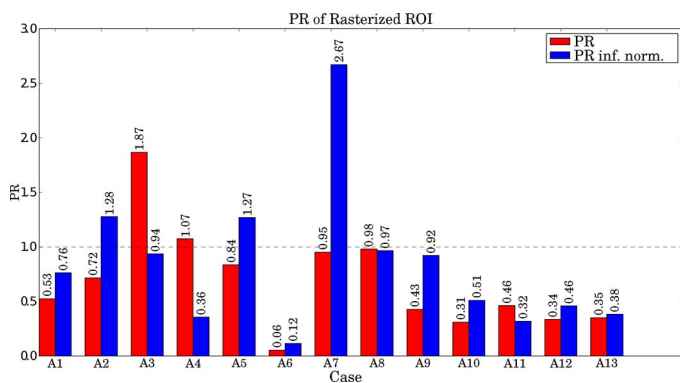


Fig. 11. Bar chart of  $\mathbf{PR}_{\text{sac}}$  (red) and  $\mathbf{PR}_{\text{sac}}^{\text{norm}}$  (blue) for all 13 pairs of DSA series (A1-A13) derived from rasterized ROIs (cf. Fig. 8(a)). A value above 1 corresponds to an increase in pulsatility after FD deployment, while a value below 1 corresponds to a decrease. Please refer to the electronic version of this article for color figures.

aneurysms where the pulsatility ratio was markedly increased after treatment (cf. Fig. 8(a) and (b) and Table III).

The same experiment was successfully repeated with rasterized ROIs (cf. Fig. 6).  $\mathbf{PR}_{\text{sac}}$ ,  $\mathbf{PR}_{\text{prox}}$ , and  $\mathbf{PR}_{\text{sac}}^{\text{norm}}$  computed from the pulsatility  $\mathbf{P}$  in the aneurysm and parent artery before and after FD deployment, respectively, are also given in Table III. The average value of  $\mathbf{PR}_{\text{sac}}$  was 0.68, the median 0.53 (SD 0.45). In case of  $\mathbf{PR}_{\text{sac}}^{\text{norm}}$ , the average was 0.84 and the median 0.76 (SD 0.64). A comparison of  $\mathbf{PR}_{\text{sac}}$  and  $\mathbf{PR}_{\text{sac}}^{\text{norm}}$  derived from rasterized ROIs can be visually assessed in Fig. 11.

In comparison to the same ratios derived from un rasterized ROIs (cf. Table III), mean and median were significantly closer to each other. Also, the standard deviations were markedly

smaller. Both pulsatility ratios indicated a significant reduction in pulsatility after FD treatment.

The cases A5 and A6, whose pulsatility ratios were strong outliers in case of un rasterized ROIs, were brought down to reasonable levels. Cases A2 and A4 which seemed to be problematic with respect to un rasterized ROIs could be regarded as being inconspicuous. In case A7, however, pulsatility measurements in the parent artery seemed to be implausibly high. As was the case when using un rasterized ROIs, case A10 and A11 share the same trend, but differ in their actual ratios.

The DSA series corresponding to case A8 is interesting due to its angulation. The contrasted parent artery is superimposed onto most of the aneurysm sac. However, the overlap is different from, for example, case A5 [cf. Fig. 9(a)]. The aneurysm in case A8 seems to almost coincide with the parent artery that is overlaid without an interruption (unlike in case A5). Both  $\mathbf{PR}_{\text{sac}}$  and  $\mathbf{PR}_{\text{sac}}^{\text{norm}}$  (and therefore  $\mathbf{PR}_{\text{prox}}$ ) are close to 1 (0.98 and 0.97). When employing un rasterized ROIs, this was not the case.

As a comparison of the various methods that can be employed in order to obtain a pulsatility ratio, Fig. 12 gives several box plots. Box plots of  $\mathbf{PR}_{\text{sac}}$  and  $\mathbf{PR}_{\text{sac}}^{\text{norm}}$  obtained from un rasterized ROIs and rasterized ROIs in the 13 cases (A1-A13) are shown.

## B. Discussion

Overall, the obtained results encourage to further investigate the change in pulsatility variations before and after FD deployment. Before discussing the results in detail, it is important to comment on the datasets that were studied.

Most importantly, the DSA series used in the experiments were not specifically acquired for this purpose. Therefore, little was assumed about the exact acquisition procedure. For instance, the heart rate of the patient at the time of acquisition was unknown. Of course, the heart rate is an important parameter in the proposed technique. To overcome this predicament and in order to cover a variety of different heart rates, the same (wide) frequency band was used in all 13 pairs of DSA series. This can likely be improved. For future experiments, it is thus desirable to record the patient's heart rate at the time of acquisition. As patients are routinely monitored for heart rate during the procedure, this information could be obtained at little cost and without affecting the therapeutic effects of the intervention in a negative way. In case of a known heart rate, the frequency band at which the various periodograms are compared could be made adaptive. Such a modification is likely to be useful when considering different cases, but might also be beneficial in patients where the heart rate differs before and after treatment. Incorporation of the true heart rate leads to an increase in patient specificity of the proposed quantity. Therefore, we would indeed expect robustness and performance to increase in this scenario.

Another factor that might be crucial, but could not be defined *a priori* and specifically to comply with the requirements of the experiments at hand, is the contrast agent injection protocol. For the proposed method, it would be favorable to deliver just a small amount of contrast agent over a long time period. In the presented study, a constant injection rate of 5 mL/s over 2 s at

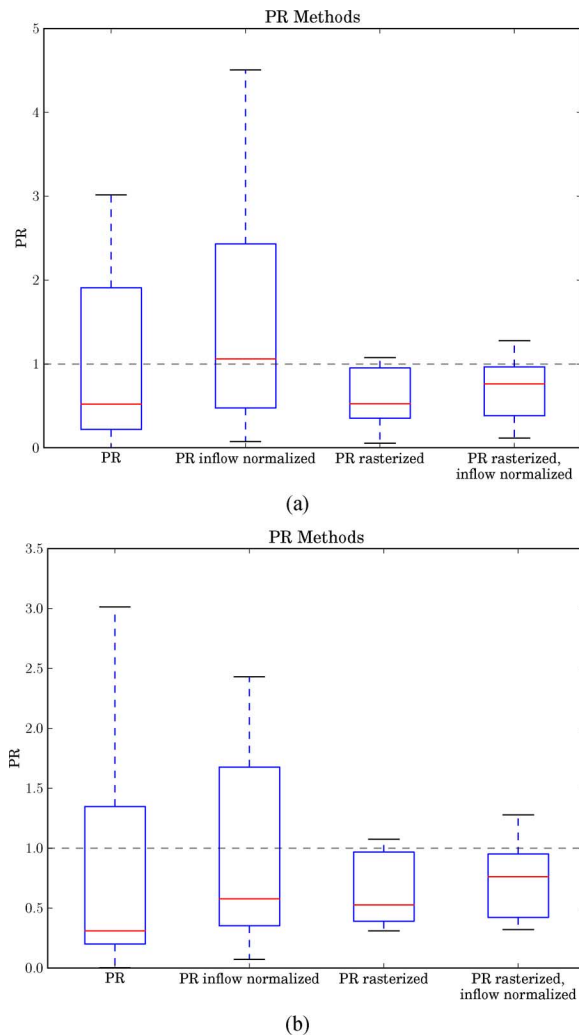


Fig. 12. Box plots of  $\mathbf{PR}_{\text{sac}}$  and  $\mathbf{PR}_{\text{sac}}^{\text{norm}}$  obtained from unrasterized ROIs and  $\mathbf{PR}_{\text{sac}}$  and  $\mathbf{PR}_{\text{sac}}^{\text{norm}}$  obtained from rasterized ROIs (cf. Table III). In (a), all cases A1-A13 were included while in (b), the cases A5 and A6 were omitted. Shown is the lower quartile Q1, the median Q2, the upper quartile Q3 and the largest ratio still within  $1.5 \cdot \text{IQR}$  ( $\text{IQR} = \text{Q3} - \text{Q1}$ ). Outliers are not shown. The effect of omitting the outliers [cases A5 and A6, cf. Fig. 8(a)] is particularly large in case of ratios derived from unrasterized ROIs. (a) From left to right: box plots of  $\mathbf{PR}_{\text{sac}}$  and  $\mathbf{PR}_{\text{sac}}^{\text{norm}}$  obtained from unrasterized ROIs and  $\mathbf{PR}_{\text{sac}}$  and  $\mathbf{PR}_{\text{sac}}^{\text{norm}}$  obtained from rasterized ROIs. (b) Same as (a), but with cases A5 and A6 removed.

300 pci pressure was used and resulted in signals exhibiting significant pulsatility. A lower injection rate (e.g., only 2 mL/s in the internal carotid artery [28]) was proposed by different sites. When using higher injection rates, signal variation is prone to be reduced due to saturation and temporary disruption of pulsatility [42]. For future studies, an automated injection with a high degree of reproducibility and a low injection rate is advisable. A comparably minor factor, but still one that needs to be considered, is the location of the catheter tip during contrast agent injection. The injection site should be sufficiently far away to guarantee good mixing of contrast medium and blood [43]. Furthermore, an injection site that is too close to the investigated ROI is likely to influence the measured blood flow significantly. While prospective *in vivo* studies are most desirable, modifications to the DSA acquisition protocol that may potentially affect the patient or operator safety or the therapeutic intervention and

its outcome must be carefully made and adhere to ethical standards for responsible medical practice.

Finally, the number and selection of the DSA series used during the experiments itself is disadvantageous for deriving quantities that could stand-up against scrutinizing. The wide diversity of aneurysms in the cohort studied here was, however, deliberately chosen. To get a first impression of what a technique might be capable of, this is certainly permissible. Still, the number of data points and their broad scattering should be reconsidered if, in the future, it is desired to evaluate the technique with respect to specific parameters.

These initial remarks were made to outline some general limitations that should be considered when studying the results that have been presented above. The results obtained from the experiments at hand are likely to be biased towards many different interfering variables and should be met with scepticism. This, however, does not necessarily dispute their usefulness. They are surely good enough to show a rough trend of whether or not this is a worthwhile direction for future research.

At first sight, the results from the experiment with unrasterized ROIs may appear discouraging (cf. Table III). A mean value of 6.09 for  $\mathbf{PR}_{\text{sac}}^{\text{norm}}$  is far from being an expected, plausible result. Upon closer inspection, especially when assessing Fig. 8(a), it becomes clear that the distribution of pulsatility ratios is strongly skewed towards higher ratios. The results further suggest that the observed skewness is mainly caused by just two cases, namely A5 and A6. Cases A5 and A6 produced results that were an order of magnitude larger than the rest. In light of this large gap, A5 and A6 can be reasonably regarded as outliers. When removing A5 and A6 from the statistical analysis, the standard deviations decreased greatly, mean and average approached each other and mostly fell into regions below 1. Cases A5 and A6 can confidently be regarded as being special with respect to the anatomy of the pictured aneurysm or the angulation of the DSA series.

A TCC extracted from the ROI inside the aneurysm corresponding to A5 is most certainly strongly influenced by superimposed vascular structures. Only a small percentage of the 2-D surface of the projected aneurysm sac seems to be clear of other vessels. In this case, averaging TCCs of each pixel in the aneurysm ROI in order to obtain a TCC that represents the ROI as an entity, seems futile. Different pixels in such an ROI are prone to exhibit a significantly different behavior. In particular, imposing a constant phase assumption on the TCCs of various pixels can, in case of A5, hardly be justified.

The aneurysm pictured in the DSA series of case A6 is the largest that was studied in the presented experiments. In case of an ROI that covers a very large region, the constant phase assumption for the TCCs of the pixels contained in the ROI is likely to be violated. In general, a shift in phase is to be expected in case of TCCs that are extracted from locations that are set apart spatially. Besides on the distance, the mismatch in phase also depends on the blood velocity. In case of fast flows, the spatial distance can be rather large while still maintaining a good agreement in phase. Inside giant aneurysms, however, the propagation speed of contrast agent would be expected to decrease in a nonlinear manner from the aneurysm neck towards outer regions of the aneurysm sac. In addition, signal pulsatility in itself is likely to be different in areas further away from the

ostium. Therefore, averaging in time domain could well be regarded as unfortunate in cases A5 and A6.

These remarks seem to be supported by the results obtained from the same analysis using rasterized ROIs. Here, case 5 is inconspicuous. Case 6, on the other hand, could now be regarded as an outlier in the opposite direction. Also, much of the reason for the high ratios in case of A5 and A6 seemed to be grounded in the inflow normalization step. It is suggested that a rasterization of ROIs has a significant effect on very large ROIs and ROIs that stem from DSA angulations of aneurysms that are strongly affected by superimposed structures.

In general, the results when using rasterized ROIs were more plausible than for unrasterized ones. Mean and average values all were markedly smaller than 1. This corresponds to a significant decrease in pulsatility after FD treatment.

Inflow normalization apparently affects the pulsatility ratio; however, a general trend whether it increases or decreases  $\mathbf{PR}_{\text{sac}}$  is not apparent. This is not surprising since the pulsatility ratio in the parent artery is expected to change independently of the case. It is rather unexpected, however, that the correlation between the effect of inflow normalization on each aneurysm in the rasterized and unrasterized case is poor. For instance, an increase after inflow normalization in the unrasterized case does not predict the same increase, or even an increase at all, in the rasterized case (and vice versa).

In general, the pulsatility estimates in the parent artery were surprisingly diverse and in some cases implausibly high or low. Differences in the size and location of the ROIs in the pre- and post-treatment DSA series could have a larger impact on the ROIs on the parent artery, which are generally smaller than their counterparts inside the aneurysm. Furthermore, ROIs on the parent artery might be more susceptible to changes in parameters related to the flow conditions. Even though the inflow normalization step was incorporated to account for changes in the parent artery, some changes might be of a nature that permits a capturing by the proposed technique. On the other hand, an average  $\mathbf{PR}_{\text{prox}}$  value of 0.99 allows for drawing a different conclusion.

Resorting to the analysis of individual cases, the aneurysms corresponding to the cases A1, A4, and A7 are of particular interest. As pointed out in Section IV, all three belong to a group that exposed significant increase in pulsatility after FD deployment. Furthermore, in all cases, image artifacts due to endovascular devices are visible. In case of A1,  $\mathbf{PR}_{\text{sac}}$  was reasonable, however, the inflow normalization step seemed to be problematic. This result can be considered as being in accordance with the fact that a catheter is visible in the parent artery during the acquisition of the post-treatment DSA series. In cases A4 and A7, a medical device seems to protrude into the inside of the respective aneurysm. Therefore, both  $\mathbf{PR}_{\text{sac}}$  and  $\mathbf{PR}_{\text{sac}}^{\text{norm}}$  should be expected to be influenced by this interference. When using unrasterized ROIs, case A7 seems to be less affected than A4. This could be explained by the much larger size of the aneurysm in case A7. When using rasterized ROIs,  $\mathbf{PR}_{\text{sac}}$  for cases A1, A4, and A7 retreated to plausible levels. This might indicate that the proposed technique is more robust towards such variations

when using rasterized ROIs. From a theoretical standpoint, this is well justified.

The aneurysm, or rather the angulation of the C-arm device during the DSA run, in case A8 is remarkable as well. Due to the angulation, the aneurysm almost completely coincides with the parent artery.  $\mathbf{PR}_{\text{sac}}$  and  $\mathbf{PR}_{\text{sac}}^{\text{norm}}$  are almost 1 in case of rasterized ROIs. Effectively, this means that neither the pulsatility inside the aneurysm nor the pulsatility in the parent artery, proximal to the aneurysm, changed. While it might not be desirable when aiming for a predictive quantity, the result can be considered plausible. Due to the angulation, a distinction between the aneurysm and the parent artery is conceivably hard to make. Therefore, measuring similar values in the aneurysm and the parent artery seems reasonable. This result should not imply that the FD treatment did not induce changes that can lead to aneurysm occlusion. This means that the proposed technique might be insensitive to the differences between pre- and post-treatment series and thus be regarded as inapplicable to similar cases. By their very nature, image-based approaches to FD treatment evaluation are limited in their detection capabilities. For instance, biochemical parameters might be equally important or even outweigh flow-related parameters which are accessible via methods like the one presented.

One rather discouraging result is related to cases A10 and A11. Since they are based on the same biplane DSA runs, one would expect a very good agreement between the pulsatility ratios derived from those cases. In both cases of rasterized and unrasterized ROIs, the computed quantities of cases A10 and A11 share the same trend. The actual values, however, do differ. It is of note that the corresponding aneurysm is very small and that the angulation in case A10 is unfavorable. In comparison to the DSA series corresponding to A11, superimposed structures are much more prevalent in case A10. Those factors could well explain the observed differences. Still, further studies with biplane DSA acquisitions seem mandatory for determining the view dependence of the proposed methods.

While it seems possible to reason about most results, some are rather hard to assess and underline the need for further studies. Rasterization of ROIs seems to be a measure that helps in easing the constant phase assumption while still maintaining the benefit of decreased variance due to the averaging of multiple periodograms. Inflow normalization quite certainly has an impact on the measured quantities. Whether the effect is beneficial, however, remains unclear. No claims about the predictive value of any of the described methods with respect to FD treatments can be derived from the data presented here.

Further comprehensive medical studies are mandatory to investigate the diagnostic validity and therapeutic value of the proposed quantities in a clinical setting. Certainly, the value of the proposed methodology can only be established in comparison to other proposed parameters or the conventional assessment of FD treatment efficacy. A well-defined benchmark data set comprising DSA acquisition characteristics, injection protocol parameters, as well as information on the therapeutic measures undertaken and the outcome at various follow-up times would enable such comparative studies and improve the consistency of reporting statistical evaluations. To increase its validity and clinical utility, any comparison should not just be based strictly on the predictive value of a parameter but should also

relate to indication and intraoperative feasibility, with special attention to operator and patient safety.

Based on the evidence gathered in our initial pilot study and expert opinion, we would advise to preferably apply our methodology to DSA series of cases in which no further endovascular devices are present and the angulation allows for the delineation of ROIs unobstructed by other contrasted structures. Typically, this is not a major restriction since interventionalists usually optimize for such views. Nevertheless, the results also suggest that incoherently averaging the extracted signals (in frequency domain) as employed in the proposed metric derived from rasterized ROIs helps mitigate artifacts induced by sub-optimal angulations and the presence of additional endovascular devices. Positive outcome provided, we would therefore afterwards scrutinize performance in less optimal scenarios using the pulsatility ratio derived from rasterized ROIs. For the presented study, we deliberately chose to have a number of challenging cases to evaluate the performance of our method under suboptimal conditions. In a real-world setting, we expect the portion of such difficult cases to be significantly smaller.

A study combining *in silico* with *in vitro* experiments may particularly be helpful for investigating the sensitivity and reproducibility of the proposed technique. Using an *in vitro* setting with an aneurysm model would be useful for investigating the correlation of the proposed parameter with particle image velocimetry measurements (cf. [24]) obtained before and after FD placement. Employing CFD simulations *in silico* would allow to assess virtual angiographies featuring flows with arbitrary pulsatility patterns and acquisition protocols, which could systematically be varied to study the effect of the parameter changes, cf. [44], [42]. Basing the *in vitro* and *in silico* experiments on identical anatomies would also open up several possibilities for cross validation.

To improve upon the methods at hand, it could also be worthwhile to investigate other PSD estimators. Especially parametric estimators might be of advantage. A specific model describing the characteristics of beat-to-beat variations in a TCC may, when employed in combination with a suitable parametric PSD estimator, be superior to the all-purpose periodogram estimator. Another idea for future work would be to study the cross power spectral density of the TCCs derived from different ROIs (for instance, proximal and distal to an aneurysm on the parent artery, before and after FD treatment). Employing more sophisticated bolus modeling approaches in the detrending step of our preprocessing pipeline could also be advantageous, at the cost of additional assumptions placed on the shape of the bolus and thus a less universally valid procedure. When thinking one step ahead, it could also be rewarding to investigate deliberately inducing oscillating variations into TCCs by means of modulating the contrast agent injection profile [45].

## V. CONCLUSION

Predicting FD treatment outcome interventionally remains an open problem. Being an emerging treatment strategy, related research efforts are rather rare and previously suggested approaches often lack thorough clinical evaluation. Besides presenting a detailed survey on existing approaches to the

angiographic analysis of hemodynamics in cerebral aneurysms, we have proposed a novel method for addressing the angiographic assessment of FD efficacy in the treatment of cerebral aneurysms based on the frequency analysis of signals derived from DSA series. An initial feasibility study shows promising results, encouraging additional research efforts in this direction. Further prospective studies are paramount to evaluate the predictive value of the proposed parameters within a clinical setting.

## ACKNOWLEDGMENT

The authors would like to give special thanks to Dr. S. Çekirge, Hacettepe University Hospital, Ankara, Turkey, for providing clinical data and expert feedback, Dr. D. Lopes, Rush University Medical Center, Chicago, IL, USA, for providing image data and expert feedback, and Dr. J. Bauer, Klinikum rechts der Isar der TUM, Munich, Germany for providing expert knowledge.

## REFERENCES

- [1] J. Suarez, R. Tarr, and W. Selman, "Aneurysmal subarachnoid hemorrhage," *N. Eng. J. Med.*, vol. 354, no. 4, pp. 387–396, 2006.
- [2] S. C. Johnston, S. Selvin, and D. R. Gress, "The burden, trends, and demographics of mortality from subarachnoid hemorrhage," *Neurology*, vol. 50, no. 5, pp. 1413–1418, 1998.
- [3] W. E. Dandy, "Intracranial aneurysm of the internal carotid artery: Cured by operation," *Ann. Surg.*, vol. 107, no. 5, p. 654, 1938.
- [4] G. Guglielmi, F. Viñuela, J. Dion, and G. Duckwiler, "Electrothrombolysis of saccular aneurysms via endovascular approach: Part 2: Preliminary clinical experience," *J. Neurosurg.*, vol. 75, no. 1, pp. 8–14, 1991.
- [5] A. Molyneux *et al.*, "Risk of recurrent subarachnoid haemorrhage, death, or dependence and standardised mortality ratios after clipping or coiling of an intracranial aneurysm in the international subarachnoid aneurysm trial (ISAT): Long-term follow-up," *Lancet Neurol.*, vol. 8, no. 5, p. 427, 2009.
- [6] K. Alfke, T. Straube, L. Dörner, H. M. Mehdorn, and O. Jansen, "Treatment of intracranial broad-neck aneurysms with a new self-expanding stent and coil embolization," *Am. J. Neuroradiol.*, vol. 25, no. 4, pp. 584–591, 2004.
- [7] D. Fiorella, M. Kelly, and H. Woo, "Flow diversion for intracranial aneurysm treatment," *Endovascular Today*, vol. 8, no. 5, pp. 67–74, 2009.
- [8] B. Lieber, V. Livescu, L. Hopkins, and A. Wakhloo, "Particle image velocimetry assessment of stent design influence on intra-aneurysmal flow," *Ann. Biomed. Eng.*, vol. 30, no. 6, pp. 768–777, 2002.
- [9] I. Szikora, P. Nelson, Z. Berentei, Z. Kulcsar, M. Marosfoi, and A. Berez, "The potential of flow modification in the treatment of intracranial aneurysms," *Intervent. Neuroradiol.*, vol. 14, no. s1, p. 77, 2008.
- [10] M. Ohta, S. Wetzel, P. Dantan, C. Bachelet, K. Lovblad, H. Yilmaz, P. Flaud, and D. Rüfenacht, "Rheological changes after stenting of a cerebral aneurysm: A finite element modeling approach," *Cardiovasc. Intervent. Radiol.*, vol. 28, no. 6, pp. 768–772, 2005.
- [11] G. Wong, M. Kwan, R. Ng, S. Yu, and W. Poon, "Flow diverters for treatment of intracranial aneurysms: Current status and ongoing clinical trials," *J. Clin. Neurosci.*, vol. 18, no. 6, pp. 737–740, 2011.
- [12] P. Lylyk, C. Miranda, R. Ceratto, A. Ferrario, E. Scrivano, H. Luna, A. Berez, Q. Tran, P. Nelson, and D. Fiorella, "Curative endovascular reconstruction of cerebral aneurysms with the pipeline embolization device: The buenos aires experience," *Neurosurgery*, vol. 64, no. 4, pp. 632–643, 2009.
- [13] I. Grunwald, M. Kamran, R. Corkill, A. Kühn, I. Choi, S. Turnbull, D. Dobson, K. Fassbender, D. Watson, and M. Gounis, "Simple measurement of aneurysm residual after treatment: The smart scale for evaluation of intracranial aneurysms treated with flow diverters," *Acta Neurochirurgica*, vol. 154, no. 1, pp. 21–26, 2011.
- [14] H. Tenjin, F. Asakura, Y. Nakahara, K. Matsumoto, T. Matsuo, F. Urano, and S. Ueda, "Evaluation of intraneurysmal blood velocity by time-density curve analysis and digital subtraction angiography," *Am. J. Neuroradiol.*, vol. 19, no. 7, pp. 1303–1307, 1998.

- [15] F. Asakura, H. Tenjin, N. Sugawa, S. Kimura, and F. Oki, "Evaluation of intra-aneurysmal blood flow by digital subtraction angiography: Blood flow change after coil embolization," *Surg. Neurol.*, vol. 59, no. 4, pp. 309–318, 2003.
- [16] Z. Wang, C. Ionita, S. Rudin, K. Hoffmann, A. Paxton, and D. Bednarek, "Angiographic analysis of blood flow modification in cerebral aneurysm models with a new asymmetric stent," in *Proc. SPIE Med. Imag., Physiol., Funct., Structure From Med. Images*, 2004, vol. 5369, pp. 307–318.
- [17] Z. Wang, K. Hoffmann, Z. Wang, S. Rudin, L. Guterman, and H. Meng, "Contrast settling in cerebral aneurysm angiography," *Phys. Med. Biol.*, vol. 50, no. 13, p. 3171, 2005.
- [18] C. Ionita, A. Paciorek, K. Hoffmann, D. Bednarek, J. Yamamoto, J. Kolega, E. Levy, L. Hopkins, S. Rudin, and J. Mocco, "Asymmetric vascular stent feasibility study of a new low-porosity patch-containing stent," *Stroke*, vol. 39, no. 7, pp. 2105–2113, 2008.
- [19] C. N. Ionita, W. Wang, D. R. Bednarek, and S. Rudin, "Assessment of contrast flow modification in aneurysms treated with closed-cell self-deploying asymmetric vascular stents (SAVS)," in *Proc. SPIE Med. Imag., Biomed. Appl. Molecular, Struct., Funct. Imag.*, 2010, vol. 7626, p. 762601.
- [20] C. Ionita, A. Paciorek, A. Dohatcu, K. Hoffmann, D. Bednarek, J. Kolega, E. Levy, L. Hopkins, S. Rudin, and J. Mocco, "The asymmetric vascular stent efficacy in a rabbit aneurysm model," *Stroke*, vol. 40, no. 3, pp. 959–965, 2009.
- [21] T. Struffert, S. Ott, M. Kowarschik, F. Bender, E. Adamek, T. Engelhorn, P. Göllitz, S. Lang, C. M. Strother, and A. Doerfler, "Measurement of quantifiable parameters by time-density curves in the elastase-induced aneurysm model: First results in the comparison of a flow diverter and a conventional aneurysm stent," *Eur. Radiol.*, vol. 23, no. 2, pp. 521–527, 2013.
- [22] C. Sadasivan, B. Lieber, M. Gounis, D. Lopes, and L. Hopkins, "Angiographic quantification of contrast medium washout from cerebral aneurysms after stent placement," *Am. J. Neuroradiol.*, vol. 23, no. 7, pp. 1214–1221, 2002.
- [23] C. Sadasivan, L. Cesar, J. Seong, A. Rakian, Q. Hao, F. Tio, A. Wakhloo, and B. Lieber, "An original flow diversion device for the treatment of intracranial aneurysms evaluation in the rabbit elastase-induced model," *Stroke*, vol. 40, no. 3, pp. 952–958, 2009.
- [24] A. Trager, C. Sadasivan, J. Seong, and B. Lieber, "Correlation between angiographic and particle image velocimetry quantification of flow diverters in an in vitro model of elastase-induced rabbit aneurysms," *J. Biomechan. Eng.*, vol. 131, no. 3, p. 034506, 2009.
- [25] C. Sadasivan, "Angiographic assessment of flow diverters as treatment for cerebral aneurysms: Results in the rabbit elastase-induced aneurysm model," Ph.D. dissertation, Univ. Miami, Miami, FL, 2008.
- [26] C. Sadasivan, B. Lieber, L. Cesar, L. Miskolczi, J. Seong, and A. Wakhloo, "Angiographic assessment of the performance of flow diverters to treat cerebral aneurysms," in *Proc. 28th Annu. Int. Conf. IEEE Eng. Med. Biol. Soc.*, 2006, pp. 3210–3213.
- [27] C. Sadasivan, L. Cesar, J. Seong, A. Wakhloo, and B. Lieber, "Treatment of rabbit elastase-induced aneurysm models by flow diverters: Development of quantifiable indexes of device performance using digital subtraction angiography," *IEEE Trans. Med. Imag.*, vol. 28, no. 7, pp. 1117–1125, Jul. 2009.
- [28] L.-D. Jou and M. Mawad, "Analysis of intra-aneurysmal flow for cerebral aneurysms with cerebral angiography," *Am. J. Neuroradiol.*, vol. 33, no. 9, pp. 1679–1684, 2012.
- [29] V. M. Pereira *et al.*, "A DSA-based method using contrast-motion estimation for the assessment of the intra-aneurysmal flow changes induced by flow-diverter stents," *Am. J. Neuroradiol.*, vol. 34, no. 4, pp. 808–815, 2013.
- [30] T. Benz, M. Kowarschik, J. Endres, P. Maday, T. Redel, and N. Navab, "Estimation of contrast agent motion from cerebral angiograms for assessing hemodynamic alterations following aneurysm treatment by flow diversion," in *XIII Mediterranean Conference on Medical and Biological Engineering and Computing 2013*. New York: Springer, 2014, pp. 475–478.
- [31] D. Roy, G. Milot, and J. Raymond, "Endovascular treatment of unruptured aneurysms," *Stroke*, vol. 32, no. 9, pp. 1998–2004, 2001.
- [32] L. Fencil, K. Doi, K. Chua, and K. Hoffman, "Measurement of absolute flow rate in vessels using a stereoscopic DSA system," *Phys. Med. Biol.*, vol. 34, no. 6, p. 659, 2000.
- [33] J. Fitzpatrick, "The existence of geometrical density-image transformations corresponding to object motion," *Comput. Vis., Graph., Image Process.*, vol. 44, no. 2, pp. 155–174, 1988.
- [34] R. Wildes, M. Amabile, A. Lanzillotto, and T. Leu, "Recovering estimates of fluid flow from image sequence data," *Comput. Vis. Image Understand.*, vol. 80, no. 2, pp. 246–266, 2000.
- [35] T. Liu and L. Shen, "Fluid flow and optical flow," *J. Fluid Mechan.*, vol. 614, no. 253, p. 1, 2008.
- [36] T. Corpetti, É. Mémin, and P. Pérez, "Dense fluid flow estimation IRISA," Tech. Rep. 135, 2000.
- [37] T. Corpetti, É. Mémin, and P. Pérez, "Dense estimation of fluid flows," *Pattern Anal. Machine Intell.*, vol. 24, no. 3, pp. 365–380, 2002.
- [38] D. Suter, "Motion estimation and vector splines," in *Proc. IEEE Comput. Soc. Conf. Comput. Vis. Pattern Recognit.*, 1994, vol. 6, pp. 939–942.
- [39] A. Crummy *et al.*, "Computerized fluoroscopy: Digital subtraction for intravenous angiocardiology and arteriography," *Am. J. Roentgenol.*, vol. 135, no. 6, pp. 1131–1140, 1980.
- [40] P. Stoica and R. Moses, *Spectral Analysis of Signals*. Upper Saddle River, NJ: Pearson/Prentice Hall, 2005.
- [41] R. Lyons, *Understanding Digital Signal Processing*. Upper Saddle River, NJ: Pearson, 2010.
- [42] M. D. Ford, G. R. Stuhne, H. N. Nikolov, D. F. Habets, S. P. Lownie, D. W. Holdsworth, and D. A. Steinman, "Virtual angiography for visualization and validation of computational models of aneurysm hemodynamics," *IEEE Trans. Med. Imag.*, vol. 24, no. 12, pp. 1586–1592, Dec. 2005.
- [43] B. Lieber, C. Sadasivan, Q. Hao, J. Seong, and L. Cesar, "The mixability of angiographic contrast with arterial blood," *Med. Phys.*, vol. 36, no. 11, pp. 5064–5078, 2009.
- [44] J. Endres, T. Redel, M. Kowarschik, J. Hutter, J. Hornegger, and A. Doerfler, "Virtual angiography using CFD simulations based on patient-specific parameter optimization," in *Proc. 9th IEEE Int. Symp. Biomed. Imag.*, 2012, pp. 1200–1203.
- [45] D. Holdsworth, M. Drangova, and A. Fenster, "Quantitative angiographic blood-flow measurement using pulsed intra-arterial injection," *Med. Phys.*, vol. 26, no. 10, pp. 2168–2175, 1999.